

- cules and the Solid State*, edited by P.-O. Löwdin (Academic, New York, 1966), pp. 157-168.
- ¹²R. A. Moore and S. H. Vosko, *Can. J. Phys.* **46**, 1425 (1968).
- ¹³S. D. Mahanti and T. P. Das, *Phys. Rev. B* **3**, 1599 (1971), and references to their previous works.
- ¹⁴P. Hohenberg and W. Kohn, *Phys. Rev.* **136**, B864 (1964).
- ¹⁵H. Brooks and F. S. Ham, *Phys. Rev.* **112**, 344 (1958).
- ¹⁶T. Kjeldaa and W. Kohn, *Phys. Rev.* **101**, 66 (1956).
- ¹⁷W. Prokofjew, *Z. Physik* **58**, 255 (1929).
- ¹⁸J. Mann (private communication).
- ¹⁹V. Fock and M. J. Petrashen, *Physik. Z. Sowjetunion* **6**, 368 (1934); **8**, 547 (1935).
- ²⁰D. A. Goodings, *Phys. Rev.* **123**, 1706 (1961).
- ²¹M. Fox and I. I. Rabi, *Phys. Rev.* **48**, 746 (1935).
- ²²P. Kusch and H. Taub, *Phys. Rev.* **75**, 1477 (1949).
- ²³W. D. Knight, *Solid State Phys.* **2**, 93 (1956).
- ²⁴J. Callaway, *Energy Band Theory* (Academic, New York, 1964), p. 155.
- ²⁵H. Brooks (unpublished) quoted by G. B. Benedek and T. Kushida, *J. Phys. Chem. Solids* **5**, 241 (1958).
- ²⁶E. T. Michah, G. M. Stocks, and W. H. Young, *J. Phys. C* **2**, 1653 (1969); **2**, 1661 (1961).
- ²⁷S. D. Mahanti, L. Ferlikkis, and T. P. Das, in *Magnetic Resonance* (Plenum, New York, 1970), pp. 91-118.
- ²⁸L. E. Drain, *Met. Rev.* **12**, 195 (1967).
- ²⁹Ch. Ryter, *Phys. Letters* **4**, 69 (1963).
- ³⁰R. I. Beecroft and C. A. Swenson, *J. Phys. Chem. Solids* **18**, 329 (1961).
- ³¹S. Schultz (private communication).
- ³²G. B. Benedek and T. Kushida, *J. Phys. Chem. Solids* **5**, 241 (1958).
- ³³D. Pines, in *Solid State Physics*, edited by F. Seitz, D. Turnbull, and H. Ehrenreich (Academic, New York, 1955), Vol. 1.
- ³⁴M. M. Pant and B. Y. Tong (unpublished).
- ³⁵M. M. Pant and B. Y. Tong, *Phys. Letters A* **36**, 133 (1971).

de Haas-van Alphen Effect in Iridium[†]

J. J. Grodski* and A. E. Dixon

Physics Department, University of Waterloo, Waterloo, Ontario, Canada

(Received 24 February 1972)

Measurements of the de Haas-van Alphen (dHvA) extremal areas have been performed in three main symmetry planes of an Ir single crystal using magnetic fields up to 120 kG. A newly designed modulation-technique magnetometer was used in modulation and sample-rotation experiments; some measurements used the torque technique. Large torque or magnetization oscillations were observed from all four closed sheets of the Fermi surface predicted by the band-structure calculations of Andersen and Mackintosh. The measured cross-sectional areas of two hole sheets centered at X in the Brillouin zone and called $X3$ and $X4$ were found to be, respectively, 30% smaller and 6% larger than the calculated ones. The observed areas of two electron sheets centered at Γ were larger than the calculated ones by not more than 0.5%. The results agree with magnetoresistance data, confirming that Ir is an uncompensated metal and that its Fermi surface does not support open orbits. A few effective-mass values were determined from torque and modulation measurements of the temperature dependence of the amplitude of dHvA oscillations in magnetic fields up to 21 kG. A simultaneous determination of effective masses associated with two dHvA frequencies beating with each other was obtained. A spin-splitting zero was observed in the $\Gamma6$ sheet in the (111) plane. The Dingle temperature was determined from the magnetic field dependence of the amplitude of torque oscillations. A generalized formula describing the magnetoresistance of an uncompensated metal was used to calibrate a copper-wire magnetoresistor for magnetic field measurements.

I. INTRODUCTION

Iridium and its face-centered-cubic (fcc) neighbors in the Periodic Table, Rh, Pt, and Pd, have recently been studied with the aim of explaining some of their unusual properties. There is considerable interest in the observed weakening of superconductivity towards the end of the sequence Ir, Rh, Pt, Pd, as well as an increasing tendency toward ferromagnetism.¹ Also, the temperature dependence of the resistivity of dilute alloys of these metals with ferromagnetic impurities^{2,3} is

unusual. This has recently been described using a simple model for scattering of conduction electrons from localized spin-density fluctuations^{4,5} in the d band resulting from a local increase of the intra-atomic Coulomb potential around the impurities. However, it is still unclear how much the local fluctuations in the spin density and how much the band structure affect the weakening of superconductivity.⁶ For either case an accurate knowledge of the existing Fermi surfaces of the involved transition metals constitutes basic information for a quantitative explanation of such effects. While

a majority of the elements in the Periodic Table have their Fermi surfaces amply determined,⁷ iridium is only now added to the list.

Iridium belongs to the $5d$ transition series of elements, and it is a metal of the platinum family. Its electronic configuration⁸ is most probably $5d^7 6s^2$ and it has the lowest known transition temperature of all superconducting elements. This most corrosion-resistant metal is the second densest element and is very hard. It is fcc with a lattice parameter⁹ of 3.8396_3 Å at room temperature and 3.8344_1 Å at 4.2 °K.

The Fermi surface of iridium was first studied by Grodski and Dixon¹⁰ with the de Haas-van Alphen (dHvA) effect and transverse magnetoresistance using a normal magnet. Data obtained from these torque dHvA studies corresponded to the smallest hole sheet predicted by Andersen and Mackintosh.^{11,12} Recently, Hörnfeldt *et al.*¹³ obtained dHvA data on the two hole sheets of the Fermi surface of iridium using the modulation technique. Volkenshtein *et al.* reported on magnetoresistance and Hall-effect measurements¹⁴ and with the recent dHvA data¹⁵ obtained in experiments using the Faraday-force method, confirmed the previous results. The present work includes measurements at high magnetic fields and has yielded much more complete data on the extremal areas of the Fermi surface of iridium. The majority of the data was obtained from low-frequency field-modulation experiments; however, torque oscillations as well as rotation of the crystal about an axis perpendicular to the magnetic field direction were also used.

Section II presents results of the dHvA theory applicable to the present study. Section III gives the predicted Fermi surface of iridium. The experimental techniques are described in Sec. IV, while Sec. V contains experimental results and discussion. A summary is given in Sec. VI.

II. dHvA EFFECT SUMMARY

Williamson *et al.*¹⁶ calculated the oscillatory part of the free energy for a system of noninteracting electrons in a magnetic field H , at a finite temperature T and including the influence of Landau-level broadening. The resulting expression corresponding to each extremal cross-sectional area of a Fermi surface of arbitrary shape is

$$G_{\text{osc}} = 2VkT \left(\frac{eH}{2\pi c\hbar} \right)^{3/2} \left| \frac{\partial^2 A}{\partial k_H^2} \right|^{-1/2} \times \sum_{j=1}^{\infty} \frac{e^{-2\pi^2 j k T / \hbar \omega_c}}{j^{3/2} \sinh(2\pi^2 j k T / \hbar \omega_c)} \times \cos \left(j \frac{\pi g m_c^*}{2m} \right) \cos \left[2\pi j \left(\frac{c\hbar A}{2\pi e} \frac{1}{H} - \gamma \right) \mp \frac{\pi}{4} \right], \quad (1)$$

where $\omega_c = eH/cm_c^*$ is the cyclotron frequency. The energy of the system oscillates with $1/H$ at the dHvA frequency

$$F = c\hbar A / 2\pi e. \quad (2)$$

Since F is solely dependent on A , the dHvA frequencies yield information about the extremal areas of a Fermi surface. The orbital cyclotron effective mass $m_c^* = (2\pi)^{-1}(\partial A / \partial E)$ and the Dingle temperature T_D associated with a certain A may be determined by successive approximations from a study of changes in the relative amplitude a of the corresponding dHvA oscillations as a function of T and H , respectively. For the present experiments in Ir the factor $[\sinh(2\pi^2 j k T / \hbar \omega_c)]^{-1}$ in Eq. (1) can be approximated by $2e^{-2\pi^2 j k T / \hbar \omega_c}$ to an accuracy of better than 1%. Hence the first approximation to m_c^* can be extracted from the slope s of a plot of $\ln(a/T)$ against T . Such a linear plot can be described by the relation

$$a = T e^c - sT, \quad (3)$$

where c is some constant. An analogous approach yields an approximation to T_D . The term $\cos(j\pi g m_c^* / 2m)$ is due to spin splitting of the Landau levels. Provided m_c^* is known, the effective splitting factor g (or spin mass $m_s = 2m/g$) can be established at the extremal areas for which the spin-splitting term is zero, causing the dHvA signal to disappear.

III. FERMI SURFACE OF IRIDIUM

The first Brillouin zone of the fcc lattice of iridium is shown in Fig. 1, with principal symme-

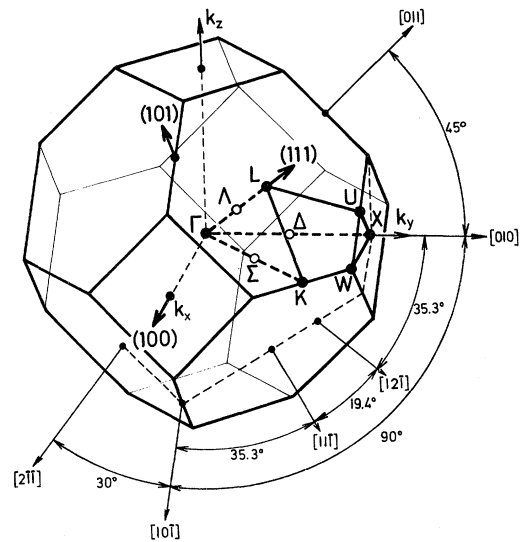


FIG. 1. Brillouin zone showing the irreducible zone of the fcc lattice and the principal symmetry points, axes, and planes.

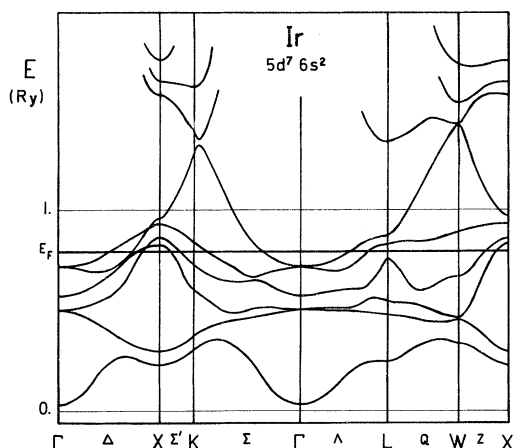


FIG. 2. Energy-band structure of iridium along the principal symmetry lines of the Brillouin zone as calculated by Andersen (Ref. 17) using the RAPW technique.

try points and axes labeled. The irreducible zone with volume equal to $\frac{1}{48}$ of the volume of the Brillouin zone is also presented in the figure. The band structure of $5d^7 6s^2$ iridium is shown in Fig. 2. It was constructed by Andersen¹⁷ from eigenvalues at the symmetry points obtained in a relativistic-augmented-plane-wave (RAPW) calculation and by relying on similarities with the band structure of Pt. The main results of the calculations however, were constant energy surfaces associated with different values of energy. The Fermi level and the resulting Fermi surface were determined^{11,12} by interpolating the energy to the value yielding a difference in volume between hole and electron sheets of one state per atom. This is appropriate since it is expected that iridium is an uncompensated¹⁸ metal as a consequence of its odd number of valence electrons and fcc structure. Figure 3 shows the (100) and (110) cross sections of the Fermi surface of iridium determined from these calculations. Following Andersen's method of labeling,¹² the Fermi surface consists of two closed electron-type sheets $\Gamma 6$ and $\Gamma 5$ and two closed hole-type sheets $X 3$ and $X 4$.

IV. EXPERIMENTAL PROCEDURE

A. Sample Preparation

The iridium sample was purchased from Koch-Light Laboratories¹⁹ and had a resistivity ratio $R_{300^\circ\text{K}}/R_{4.2^\circ\text{K}}$ of about 100. The whole crystal, about 1 in. long and $\frac{1}{8}$ in. diam, was held in its central region with a Kel-F ring for initial torque dHvA and magnetoresistance experiments. Small samples, about 10 mm^3 , were spark-cut and ac electropolished²⁰ in an aqueous potassium-cyanide solution and these were used in dHvA modulation experiments. They were aligned using Laué back-

reflection x-ray photographs and transferred²¹ to sample holders where they were glued with G. E. Glyptal cement and checked for correct alignment to within $\pm \frac{1}{2}^\circ$. No bending or distortion of the very hard samples was expected to occur as the glue dried or contracted.

B. Magnetic Fields

The first torque and field-modulation experiments were performed using a 21-kG Magnion electromagnet equipped with 12-in. alloy pole pieces tapered to 4 in. diam, and with a 2-in. air gap. The magnetic field intensity in the magnet was measured to an accuracy of 0.1% with a Rawson rotating-coil gaussmeter with a null-balance indicator incorporated into a Magnion power supply with a field-feedback control. The gaussmeter was calibrated *in situ* using another rotating-coil gaussmeter with its coil set in the geometrical center of the magnet. The reference gaussmeter was calibrated using proton NMR signals. The magnet was equipped with flat spiral modulating coils bonded to the magnet pole faces. The coils yielded a modulating field of 20 G/A of modulating current. The magnet was also equipped with a variable-speed rotation mechanism. The angular position of the magnet was monitored using a friction-driven ten-turn potentiometer.

In the next stage, two superconducting solenoids were used in field-modulation experiments. A 57-kG Westinghouse solenoid produced a magnetic field strength linearly proportional to the energizing current. The system was calibrated using

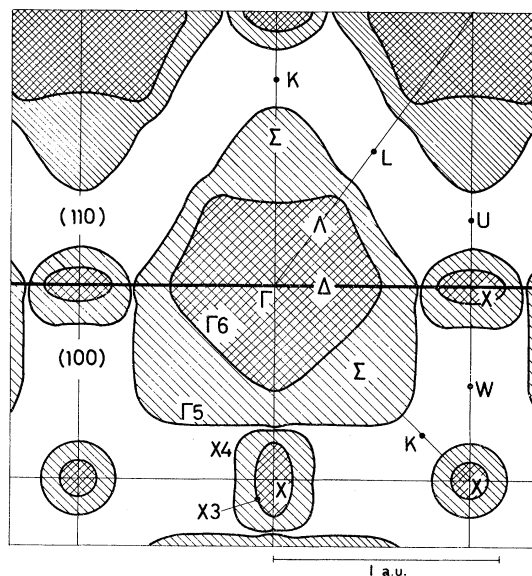


FIG. 3. Cross sections of the Fermi surface of iridium in the central (100) and (110) planes in the periodic zone scheme (Ref. 12).

NMR signals. A magnetoresistor (MR) of 3-mil-diam high-purity copper wire was used to measure the field strength in a 120-kG RCA solenoid. The MR was wound noninductively in two layers 1.6 in. long on a former that fitted between the insert Dewar and the bore of the solenoid. A constant current of 8 mA for the MR coil was supplied by a modified Kepco constant-current supply with improved stability.⁸ Calibration of the MR gaussmeter was done in two stages. The first one consisted of NMR calibration up to 47.7 kG using an Al²⁷ powder sample in which the effect of the Knight shift was taken into account. The well-known [111] belly dHvA oscillations from the Fermi surface of copper²² were used to cover the remaining field range up to a maximum of 119 kG. A total of 33 magnetic field levels with corresponding MR voltages were obtained in the two stages and they were used in a computer program designed to yield a complete calibration table allowing correlation of the MR voltages with the magnetic field values.

The program used a generalization of the expression derived by Pippard²³ for the resistivity ρ of a model metal having two spherical Fermi surfaces, one of electrons and one of holes. Pippard's expression

$$\rho = \frac{1}{\sigma} \frac{1 + \omega_c^2 \tau^2}{1 + [(n_- - n_+)/ (n_- + n_+)]^2 \omega_c^2 \tau^2}, \quad (4)$$

where n_- and n_+ are the respective numbers of electrons and holes in a unit cell and σ is the conductivity, exhibits saturation at high magnetic fields, characteristic of uncompensated metals like copper. The generalization describing the magnetoresistance of a copper MR coil had the following form:

$$\rho = \kappa \frac{1 + \xi H^\gamma}{1 + \eta H^\gamma}, \quad (5)$$

in which κ , ξ , η , and γ are constants. When the current in the MR is constant, the voltage measured across the MR coil also follows this relation. The gross effects of a copper-wire MR are well described by this equation, which also has the advantage that it can readily be inverted to yield the value of the magnetic field H when the magnetoresistance characteristics are known:

$$H = \left(\frac{\rho - \kappa}{\xi \kappa - \eta \rho} \right)^{1/\gamma}. \quad (6)$$

In order to calculate the constants in either Eq. (5) or (6), a computer program utilizing a least-squares fit was developed, yielding calibration with an accuracy of at least 0.5%. When high accuracy was required, a method using orthogonal polynomials was applied,²⁴ taking into account second-order effects exhibiting an oscillatory behavior

superimposed on a relation such as (6).

C. Torque, Field-Modulation, and Rotation Techniques

A self-balancing torque magnetometer similar to that described by Vanderkooy and Datars²⁵ was used in the torque dHvA measurements on the electromagnet. It used a Weston Inductronic amplifier²⁶ with an additional electronic amplifier⁸ providing current gain in the feedback loop. The torque from the sample was transmitted to the movable coil of the galvanometer by means of a suspension consisting of a Kel-F stirrup, a tiny aluminum universal joint, and a long quartz tube with 2-mm bore and 3-mm o.d. The universal joint consisted of two concentric rings which could rotate around mutually perpendicular axes with beryllium-copper pins as bearings. It allowed the suspension to take an unrestrained vertical position, even if the galvanometer was slightly tipped.

A large-amplitude field-modulation^{27,28} magnetometer for the electromagnet consisted of two coaxial pickup coils with identical numbers of turns of No. 32 AWG insulated copper wire. The coils were connected in series opposition. An aligned sample was located in the 0.25-in. bore of one of the coils. The samples were aligned with one of the main crystallographic planes perpendicular to the vertical magnet-rotation axis. The signal was usually detected with the angle between the axes of the steady and modulation fields up to a maximum of about $\pm 60^\circ$. At a 108-Hz modulation frequency there was complete penetration of the sample. The dHvA signal was picked up at one of the first even harmonics and detected with a phase-sensitive detector (PSD). In order to keep the natural amplitude of the dHvA signal unaffected,²⁸ the modulation was increased approximately as a function of H^2 using a manually-controlled variable-speed motor²⁹ to turn a ten-turn potentiometer connected across the oscillator output. This varied the portion of the signal controlling the modulation level. The same signal was used with a phase shifter and a transformer for bucking²⁷ the fundamental of the modulating frequency at the input to the preamplifier of the PSD. Finally, the dHvA signals in either the torque or the modulation experiments were displayed on a strip-chart recorder together with magnetic field marks at 0.5-kG intervals. Traces obtained in this way were analyzed manually.

The main features of the modulation magnetometer for use in superconducting solenoids are shown in Fig. 4. The mechanical system providing rotation of the sample in a plane perpendicular to the magnetic field direction consisted of two 0.25-in.-diam gears, one being the sample holder itself, while the second worked as an idler gear. An external 1-rpm synchronous motor was coupled

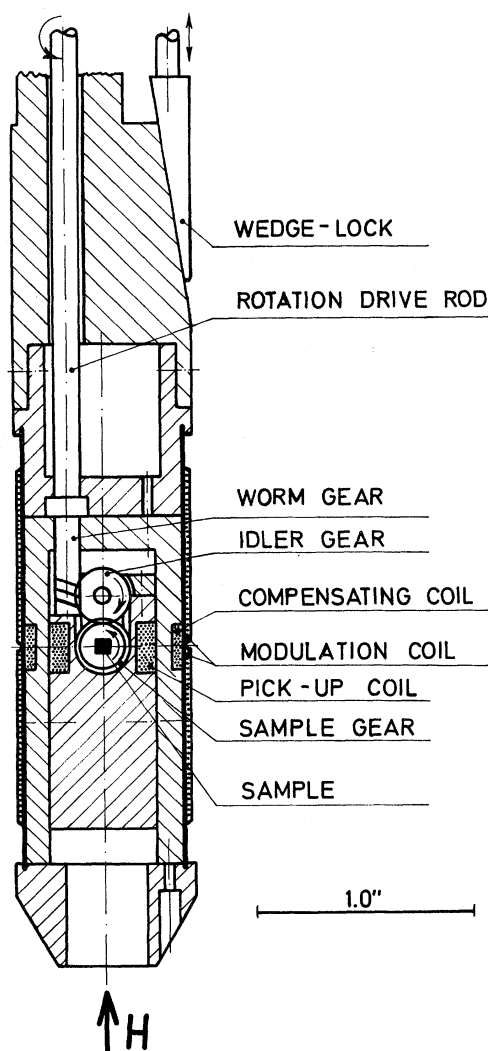


FIG. 4. Modulation magnetometer for dHvA-effect signal detection.

through a set of selectable gears and a long shaft to the worm drive. A turns counter yielded 0.1° resolution in the sample rotation while a 25-turn potentiometer monitored the continuous motion of the sample. Although backlash of about 2° was present, the relative accuracy of the readout was limited only by the resolution of the turns-counting mechanism, provided motion was in one direction only. The pickup coils wound with No. 44 AWG insulated copper wire formed a compensated²⁸ set of a concentric, coaxial design. The inner coil had 4180 turns while the outer balancing coil had 1549 turns, yielding minimum pickup of the modulation field. The system was more sensitive than a coaxial pair of coils that are not concentric.³⁰ The latter is often used since it provides space for a cylindrical sample holder which can be turned by a worm gear set external to the detection coils.

The present system was also considered to be simpler to manufacture than a spiral-gear arrangement,³¹ and it provided smooth, accurate and continuous rotation which was particularly important in the rotation technique. It had stationary pickup coils which yield signals which were free from background in the rotation experiments. This might occur in the spiral-gear arrangement where the pickup coils rotate along with the sample about an axis perpendicular to the magnetic field direction. The complete system was made of Kel-F in order to avoid differences in thermal contraction of different materials. Kel-F has the smallest thermal-expansion coefficient of the plastics group. Friction in the solid bearing surfaces at the gear shafts and in other moving parts was minimized by using molybdenum disulfide powder.³² A long and thin Helmholtz-like³³ modulation pair wound on a stainless-steel former produced a field-modulation intensity of 400 G/A. The coil consisted of 1500 turns of No. 36 AWG insulated copper wire. The former was clamped at both ends and remained rigidly fastened at all temperatures. Vibrational noise was reduced by potting all coils and leads with G. E. Varnish³⁴ and using a wedge for locking the magnetometer in the Dewar. Electronic processing used in conjunction with the 57-kG solenoid was the same as that used by Poulsen *et al.*,³⁰ and it included signal recording on magnetic tape and subsequent fast Fourier analysis for resolving dHvA spectra. However, the last part of the present work done on the 120-kG solenoid was conducted without the recording system necessitating manual analysis of the traces. In order to simplify the analysis some bandpass signal filtering was applied at the output of the PSD.

All dHvA data were taken at about 1.1°K attained by He⁴ evaporative cooling. However, accurate temperature determination was performed only in connection with the measurement of the temperature dependence of the dHvA amplitudes. A precision manometer³⁵ was used for the helium pressure determination at a level just above the helium bath.

V. EXPERIMENTAL RESULTS AND DISCUSSION

A. X-Centered Hole Sheets

Results from the modulation experiments on the electromagnet duplicated the torque data¹⁰ in the (110) plane. However, data for (100) are complementary to the torque results. Figure 5 shows the dHvA frequency plot for a sample oriented in the (100) plane. Circles indicate frequencies obtained from the torque technique while crosses correspond to results from the modulation technique. There is good agreement between the

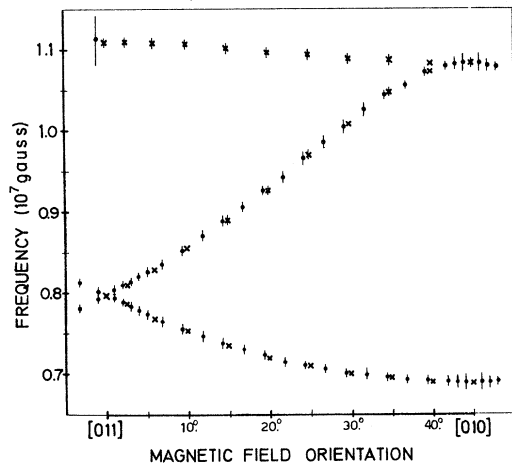


FIG. 5. Angular variation of dHvA frequencies in the (100) plane obtained on the normal magnet. Circles and crosses indicate data obtained from the torque and the modulation techniques, respectively.

torque and modulation results, however, the modulation data were particularly useful in completing the upper-most branch of frequencies. The modulation technique allows for a relatively simple enhancement of weak signals and the magnetization is not dependent on $\partial F/\partial\theta$ as is the case with the torque. Since the upper-most branch is quite flat,

the corresponding torque signals are very small. Most of the torque dHvA frequencies were obtained from traces using a magnetic field span of about 9 kG, except for a few positions close to [010] where the signals were only observed over a small field range. The $\partial F/\partial\theta$ dependence was responsible for this change, causing some data close to high-symmetry directions to be of lower signal amplitude and therefore lower accuracy. The error bars associated with the torque data illustrate this aspect. They indicate the extent of possible errors in magnetic field measurement and counting of oscillations but do not include contributions from a possible crystal misalignment of up to $\pm 1\%$. Where not indicated, the error bars were smaller than the dimensions of the symbols indicating the data points. For most of the modulation data, the extent of uncertainty of the results was smaller than $\pm 0.3\%$ of the measured dHvA frequency.

The next higher dHvA frequencies were observed in measurements on the 57-kG solenoid. With the variable modulation set to give maximum amplitude for the higher dHvA frequencies, each field sweep yielded between four and seven fundamental frequencies, two or three of which belonged to the set of frequencies observed in experiments on the electromagnet. The two resulting sets of frequencies in the three main symmetry planes (100), (101), and (111) are shown in Fig. 6. The

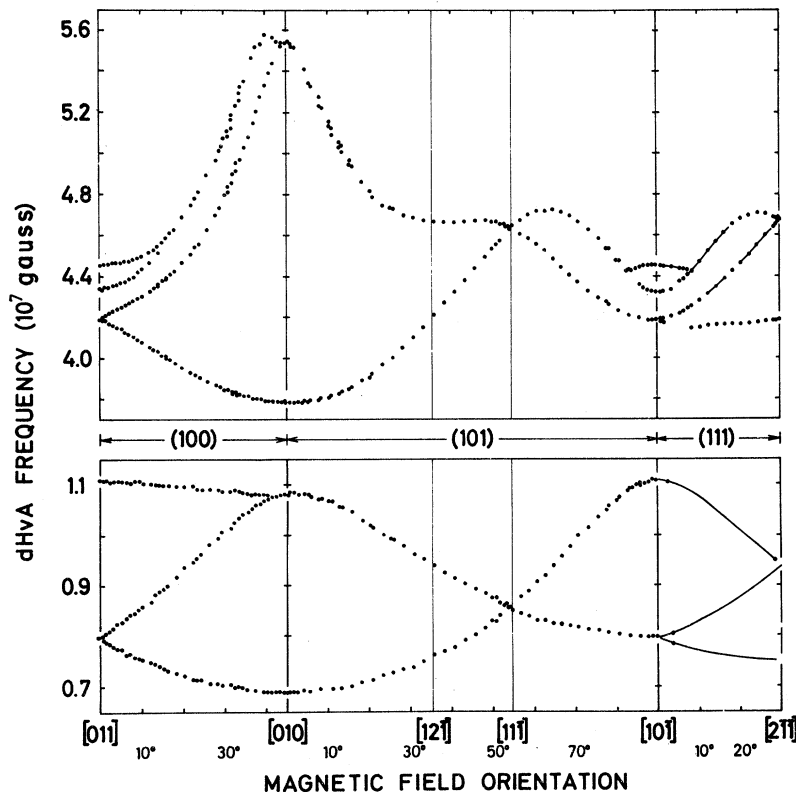


FIG. 6. Angular variation of the lower-frequency dHvA oscillations in the three principal symmetry planes. Experimental points from the "field-sweep" measurements are denoted by circles. Solid lines represent results from the rotation technique.

agreement between data obtained at the same symmetry directions but in different planes was very good indeed, as is evident from the figure. The range of the new dHvA frequencies extended from 3.8×10^7 to 5.6×10^7 G. Results for both sets in the (111) plane were obtained in the last stage of experiments on the 120-kG solenoid. The continuous lines of data shown in this plane were obtained using the rotation technique. Points shown on these lines and elsewhere were obtained from "field-sweep" measurements, and they were used for positioning the rotation data. The rotation experiments yield changes of the dHvA frequency with orientation.

A family of dHvA frequencies in each data set corresponds to several equivalent pieces constituting a Fermi-surface sheet. Each member of a set has the symmetry³⁶ of a particular characteristic point in the Brillouin zone, and the number of members in a set depends on how many times this characteristic point occurs in the zone. Simple closed Fermi sheets have corresponding dHvA frequency curves over the complete range of angles. The two sets of frequencies in Fig. 6 have the same general behavior in spite of differences in details and in the magnitude. Consequently the two Fermi sheets corresponding to the two sets of dHvA frequencies must have the same symmetry. It follows from symmetry considerations of each data set that the frequencies arise from a set of closed convex surfaces oriented along the $\langle 100 \rangle$ axes, possessing fourfold symmetry and centered at the point X of the Brillouin zone. The sheets are readily identified to correspond in the order of increasing frequencies to the hole-type $X3$ and $X4$ sheets predicted by Andersen and Mackintosh.^{11,12} No dHvA signals were recorded which would indicate the existence of a hole sheet centered at L in the Brillouin zone, as has been observed in rhodium. Thus the answer to the question about its existence¹² seems to be negative, in agreement with the results of Hörnfeldt.¹³

The shape of the $X3$ sheet is close to an ellipsoid of revolution about the ΓX line with a very slight depression in the XU directions. The shape of the $X4$ sheet is not so simple. An examination of the data corresponding to the $X4$ sheet shows splitting of dHvA frequency branches in the vicinity of $\langle 110 \rangle$. The splitting yields two extremal area values of 0.1156 and 0.1190 a.u. If a Fermi surface piece has more than one extremum, each contributes its own oscillations. The lower split branch of dHvA frequencies joins smoothly with the rest of the frequency curves, suggesting its correspondence to the central cross-sectional area. The detected strength of the higher branch was larger than that of the lower one, suggesting that the higher split branch corresponds to two

cross-sectional areas. It is easily deduced from the symmetry requirements that the splitting in the vicinity of $\langle 110 \rangle$ is indeed caused by the existence of a minimum cross-sectional area in a plane intersecting the sheet through the center point X . The other part of the split branch is due to two identical noncentral, symmetrically-set maximal areas, each arising from four bulges in the Fermi sheet. The bulges in the $X4$ sheet shown in the (100) plane in Fig. 3 considerably deform the sheet from an ellipsoidal shape. A maximum at about 65° in one of the dHvA data curves in the (101) plane, shown in Fig. 6, is also due to the bulges.

A general comparison of the experimental results with the RAPW band calculation¹¹ and with the experimental results of Hörnfeldt *et al.*¹³ and Volkenshtein *et al.*¹⁴ is given in Table I. The table contains the dHvA frequencies and the effective masses at symmetry directions. The errors indicated for data from the present work do not include contributions from a possible crystal misalignment of up to $\pm \frac{1}{2}^\circ$. There is a general agreement between the experimental results, except for the data for $X4$ at $\langle 110 \rangle$. It is expected that the difference between the cross-sectional areas in the data of Hörnfeldt *et al.*, observed as a beat, is too large. Most probably the larger value corresponds to the strong signals from the noncentral maximal areas rather than to the central minimum. The data, which did not indicate the existence of noncentral maximal areas such as were found in the present investigation, were inverted¹³ to yield Fermi radii. The resulting shape¹³ of the $X4$ sheet exhibits quite different features from those predicted by RAPW calculations.^{11,12} The theoretical data show a bulge in the $X\Gamma W$ plane in about the $X\Sigma$ direction (see Fig. 1), which produces a minimum in the $X\Gamma$ direction. The Fermi radii obtained by Hörnfeldt do not exhibit that form. At the same time there is relatively poor agreement between experimental data in the (110) plane and a line representing a fit to the expansion in spherical harmonics obtained by Hörnfeldt *et al.*¹³ The theoretical (RAPW) data predicts noncentral maxima and a central minimum. On the basis of the present experimental data, it is therefore suggested that the $X4$ sheet has basically the features predicted by the RAPW calculations but with slightly altered dimensions, as shown in Fig. 7. Although an inversion of limited accuracy is possible with data corresponding to the three main planes, inversion of the present data has been deferred until appropriate computer programs are written. The experimental area values for the $X4$ sheet are larger than the theoretical ones by an average of about 6%, while the observed $X3$ surface is approximately 30% smaller in cross-sectional

TABLE I. Comparison of calculated and measured extremal areas and cyclotron effective masses of the hole sheets in iridium.

Hole Sheet	Direction	Extremal area (a.u.)			Cyclotron mass ratio (m_c^*/m)			Enhancement ratio	
		Theory ^a	Present work	Experiment Others	Theory ^a	Present work	Experiment Others		
X3	$\langle 100 \rangle$	0.0261	0.0184 ± 0.0001	0.0183 ^b 0.0186 ^c 0.018 ^d ± 0.001	0.21	0.22 ± 0.01	0.228 ^c ± 0.003 0.22 ^d ± 0.02	1.1	
		0.0388	0.0290 ± 0.0001	0.0289 ^b 0.0293 ^c 0.029 ^d ± 0.001	0.24		0.28 ^c ± 0.01 0.27 ^d ± 0.02	1.2	
	$\langle 110 \rangle$	0.0293	0.0213 ± 0.0001	0.0213 ^b 0.0216 ^c 0.021 ^d ± 0.001	0.22	0.24 ± 0.01	0.24 ^b ± 0.025 0.26 ^c ± 0.01 0.25 ^d ± 0.02	1.1	
		0.0405	0.0297 ± 0.0001	0.0297 ^b 0.0301 ^c 0.031 ^d ± 0.001	0.26	0.32 ± 0.03	0.31 ^c ± 0.01 0.28 ^d ± 0.02	1.2	
	$\langle 111 \rangle$	0.0318	0.0229 ± 0.0002	0.0228 ^b 0.0233 ^c 0.024 ^d ± 0.001	0.22		0.25 ^c ± 0.01 0.25 ^d ± 0.02	1.1	
	$\langle 211 \rangle$		0.0201 ± 0.0001 0.0251 ± 0.0002						
	X4	$\langle 100 \rangle$	0.0915	0.1012 ± 0.0003	0.1022 ^c	0.65		0.91 ^c ± 0.02	1.4
			0.1467	0.1483 ± 0.0010	0.1497 ^c	1.05			
		$\langle 110 \rangle$	0.1065	0.1120 ± 0.0003	0.1098 ^c	0.76			
			0.1098	0.1156 ± 0.0003 $0.1190^e \pm 0.0003$	0.1178 ^c	0.72		0.97 ^c ± 0.03	1.3
$\langle 111 \rangle$		0.1164	0.1237 ± 0.0006	0.1252 ^c	0.83		1.28 ^c ± 0.02	1.5	
$\langle 211 \rangle$		0.1120 ± 0.0003 0.1249 ± 0.0006							

^aSee Ref. 11.^bSee Ref. 10.^cSee Ref. 13.^dSee Ref. 14.^eNoncentral extremal area.

tional area than the predicted one. From the present experimental data, it was calculated that the X4 set of holes contributes 0.073 ± 0.003 states/atom to the carrier concentration. This value is larger than Andersen's theoretical value of 0.0677 states/atom and smaller than Hörnfeldt's value of 0.078 ± 0.002 states/atom. In the case of the X3 set of holes the carrier concentration calculated by Hörnfeldt (0.0068 ± 0.0001 states/atom) was confirmed. However a check on the contribution of the theoretically predicted sheet revealed that a value of 0.011 states/atom would better correspond to the predicted dimensions of the sheet than the specified¹² value of 0.0093 states/atom. Summing the contributions of both the X3 and X4 sets of holes, it is found that the experimental data yield a total of about 0.081 states/atom which is larger than the theoretical value¹² by 0.004 states/atom.

The effective masses from the modulation ex-

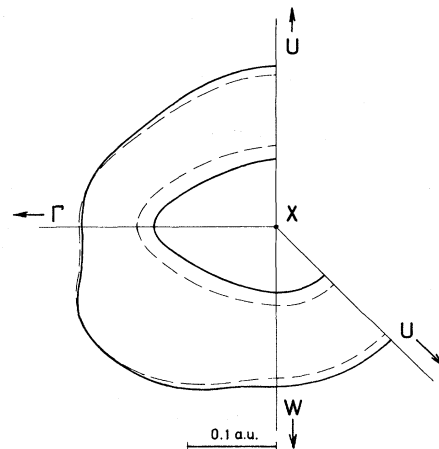


FIG. 7. Sections of the two hole pockets of iridium for three main symmetry planes. The solid lines correspond to the experimental data. The dashed lines were calculated by Andersen and Mackintosh (Ref. 11).

periments in fields up to 21 kG are also compared in Table I with the experimental data of Hörnfeldt *et al.* and the calculated¹¹ values. The measurements of the dependence of amplitude on temperature were also made using the torque technique¹⁰; however, noise due to vigorous boiling of the liquid helium above the λ point restricts the available range of temperatures and enhancement of one signal with respect to another is difficult in this technique. The modulation technique is free from such problems, which permits its wider use and yields better accuracy. However, even there it is sometimes hard to eliminate all unwanted frequencies when the frequency whose effective mass is to be measured is very weak compared to the others. If the amplitude of the envelope of the dHvA oscillations is due to two frequencies with amplitudes described by Eq. (3),

$$a_1 = T e^{c_1} r^{s_1 T} \text{ and } a_2 = T e^{c_2} r^{s_2 T}, \quad (7)$$

then the beat maxima a_{\max} and minima a_{\min} are defined, respectively, by the sum and difference of the amplitudes of the individual frequencies. Hence, it is readily shown that

$$\ln[(a_{\max} + a_{\min})/T] = c_1 - s_1 T, \quad (8)$$

$$\ln[(a_{\max} - a_{\min})/T] = c_2 - s_2 T.$$

Therefore by constructing two plots from data containing maxima and minima in the envelope of the dHvA oscillations, due to beating of two frequencies, an indication of the effective masses corresponding to both of the frequencies may be obtained. One plot would be constructed from the sums of two extremal amplitudes, while another one would use the differences of the two amplitudes. Such an approach was used with data obtained from signals detected at the twelfth harmonic of the modulation frequency at about 20 kG at [011], yielding the unknown effective-mass ratio for the frequency 1.11×10^7 G to be $m^*/m_0 = 0.32 \pm 0.03$. From Table I it is apparent that the cyclotron effective masses determined in the experiments are slightly larger than the theoretical values yielding an enhancement ratio of about 1.1 in the case of the X3 sheet, which is similar to the enhancement ratio for the analogous sheet in rhodium.¹¹

The Dingle temperature was also evaluated in the torque experiments involving signals from the X3 sheet. It was found to be $T_D = 1.3 \pm 0.1$ °K at $\langle 110 \rangle$ and estimated to be 1.1 °K at $\langle 100 \rangle$. The relatively high value is not surprising in the relatively impure (RRR=100) crystal. These values do not necessarily refer to the whole crystal since the electronic lifetimes and the associated Dingle temperatures, in general, are anisotropic. The relaxation time τ for the sample was estimated from the Dingle temperature to be 0.85×10^{-12} sec using

the relation $T_D = \hbar/2\pi k\tau$. Another estimate of the relaxation time was obtained from the relation $\tau = m/Ne^2\rho$, where m is the electronic mass, N is the density of free electrons, and ρ is the resistivity. Assuming that the two 6s electrons in the atomic configuration of iridium are free, $\tau \sim 0.5 \times 10^{-12}$ sec. The agreement between these two values is satisfactory in view of the rough assumptions.

B. Γ -Centered Electron Sheets

The next set of dHvA frequencies was obtained using the 57-kG solenoid, and it is shown in Fig. 8 for the (101) plane. An appropriately lower modulation amplitude and a magnetic field range above 51 kG were used. The measured set of frequencies clearly indicates a single branch, except for a split in the vicinity of the [111] direction. Data of such a nature are due to a largely s-like electron sheet centered on the Γ point in the Brillouin zone and called Γ_6 . The observed signals were very weak outside a range of about 30° in the vicinity of the [111] direction. This was expected since the theoretical effective mass rises¹¹ along with the rising dHvA frequencies on both sides of $\langle 111 \rangle$ from 1.34 to 1.89 at $\langle 110 \rangle$ and 1.42 at $\langle 100 \rangle$. The

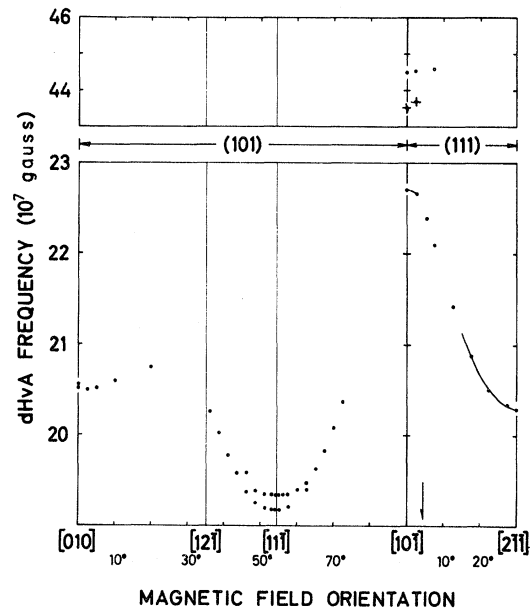


FIG. 8. Angular variation of the higher-frequency dHvA oscillations in (101) and (111) planes. Experimental points from "field-sweep" measurements are denoted by circles, while those denoted by crosses have been determined from beating oscillations and are somewhat less reliable. Solid lines represent the results from the rotation technique. The arrow in the (111) plane indicates the angular position of the spin-splitting zero observed with the lower set of frequencies.

possible existence of spin-splitting zeros on both sides of $[11\bar{1}]$ and particularly in the direction $[10\bar{1}]$ was not excluded. This would contribute to a diminishing of signal strength over a range of angles. A purer sample or higher magnetic fields would allow further data to be obtained. The observed split at $[11\bar{1}]$ yields the two values 0.5125 and 0.5169 a. u. It results from additional extremal areas due to distortions in the surface away from a spherical shape. Small bumps exist in the $\langle 111 \rangle$ directions, and consequently the smaller area at $[11\bar{1}]$ is the central section through Γ while the larger one comes from two noncentral sections across the bumps. The split is analogous to that in the corresponding Fermi-surface sheets of platinum³⁷ and palladium.³⁸ The platinum metals were predicted¹² to have very similar Γ_6 sheets; however, so far no splitting has been observed in rhodium where the presence of a large harmonic content from the hole pockets³⁹ obscured details of the Γ_6 sheet. There must also be smaller bumps in the Fermi sheet in the $\langle 100 \rangle$ directions because the extremal area at $[010]$ is larger than that at $[11\bar{1}]$. This is in agreement with the theoretical results.^{11,12}

Further experimental work using the RCA solenoid yielded the results shown in Fig. 8 in the (111) plane. The data for the Γ_6 sheet were obtained from both "field-sweep" and rotation experiments. At an angle of 4.5° from $[10\bar{1}]$, the dHvA signal disappeared at all magnetic field strengths. Andersen's value¹¹ of m_c^* for Ir at $\langle 110 \rangle$ is 1.89. Since Ir has the lowest enhancement factor¹² in the fcc platinum group of metals and since the enhancement factors for $\langle 110 \rangle$ for the Γ_6 sheets in Pd³⁸ and Pt³⁷ are 1.56 and 1.45, respectively, being slightly smaller than the average enhancement factors for the elements, the corresponding enhancement factor for Ir is expected to be about 1.25. This would yield $m_c^* \approx 2.4$ for $\langle 110 \rangle$ in Ir. The effective mass drops continuously from this value in all directions, and it is expected to have a similar form to that for the Γ_6 sheet in Pd³⁸. The spin-splitting zero at 4.5° in (111) suggests that the g factor for Ir has an anisotropy similar to that in Pd³⁸. Hence the disappearance of the signal is postulated to be due to the spin splitting corresponding to $m_c^*/m_s = 2.5$, which results in the disappearance of the $j=1$ term in the summation in Eq. (1) and yields a g factor of about 2.1.

Figure 8 also presents data in the highest dHvA frequency range which was observed in the present work, i. e., above 40×10^7 G. This set of frequencies belongs to a fourth sheet of the Fermi surface of iridium. Areas this large can only be associated with the large Γ -centered, largely d -like Γ_5 electron sheet. From the band-structure considerations,¹² it is expected that this sheet is

pulled out along the $\langle 110 \rangle$ directions. Hence the area is smaller near $[10\bar{1}]$ than at $[010]$ and at $[11\bar{1}]$. An orbit near $[010]$ would contain four of the $\langle 110 \rangle$ bumps and one near $[11\bar{1}]$ would contain six, while the $[10\bar{1}]$ orbit would contain only two. Thus $[10\bar{1}]$ would be the most favorable direction for observation of this surface.³⁹ This was indeed the case found in the experiments. The observed frequencies show a splitting which converges into a single branch at about 10° from $[10\bar{1}]$. The lower branch of frequencies was obtained from a beat pattern, and its position below the main frequency is not absolutely certain although probably it is the correct one. With the magnetic field along $[10\bar{1}]$, the observed split in the dHvA frequency yielded 1.163 a. u. for the cross-sectional area which encompasses two bumps while two identical symmetrically set noncentral areas encompass four bumps yielding a maximum of 1.189 a. u. The split in the (101) plane might reach as far as beyond the $[11\bar{1}]$ direction. From the theoretical data,¹¹ it is expected that beyond an angle of 10° from $[10\bar{1}]$ in the (111) plane, the frequency will be strongly angle dependent and will rise very steeply. A local crystal misorientation due to microstructure damage or slight bending may cause a slight angular spread in the sample. A simple calculation shows that an angular spread of as little as 0.05° in the region with steeply varying frequency may cause serious phase smearing in the dHvA signal and almost certainly this was the reason for the signal loss in that angular range.

Table II gives a comparison of the experimental results with the RAPW band calculation¹¹ for the electronlike sheets. The agreement is better than in the case of the hole sheets. The experimentally determined hole sheets were found to contribute to carrier concentration 0.004 states/atom more than the theoretical value indicated. Since the differ-

TABLE II. Comparison of calculated and measured extremal areas and cyclotron effective masses of the electron sheets in iridium.

Electron sheet	Direction	Extremal area (a.u.)		Cyclotron mass ratio (m_c^*/m) Theory ^a
		Theory ^a	Experiment	
Γ_6	$\langle 100 \rangle$	0.541	0.548 ± 0.002	1.42
	$\langle 110 \rangle$	0.607	0.6069 ± 0.0006	1.89
	$\langle 111 \rangle$	0.510	0.5125 ± 0.0006 $0.5169^b \pm 0.0006$	1.34
	$\langle 211 \rangle$		0.5426 ± 0.0006	
Γ_5	$\langle 100 \rangle$	1.507		2.55
	$\langle 110 \rangle$	1.162	1.163 ± 0.001 $1.1889^b \pm 0.0006$	2.26
	$\langle 111 \rangle$	1.448		3.02

^aSee Ref. 11.

^bNoncentral extremal area.

ence in volumes between hole and electron sheets of iridium is expected to be 1 state/atom, the theoretical value of 1.077 states/atom for the electron sheets has to be increased by the same amount, i. e., to 1.081 states/atom. Because the electron sheets are relatively large, this change in the carrier concentration should produce only a minor increase in the cross-sectional areas of the sheets. This was indeed found to be the case since the observed electron cross-sectional areas are on the average larger than the predicted ones, yet they differ only by an average of 0.5%.

A measurement of torque in a slowly rotating magnetic field in the (100) and (101) planes has not shown any large anisotropy in the magnetoresistance^{40,41} of iridium. This agrees with the transverse magnetoresistance measurements^{10,14} and the dHvA data, and it indicates that the Fermi surface of iridium does not support open orbits. A tendency toward saturation of the magnetoresistance^{10,14} at higher magnetic fields as well as the dHvA data confirm that iridium is an uncompensated¹⁸ metal.

VI. SUMMARY

Low-field torque measurements yielded data from the smallest sheet X3 of the Fermi surface. The modulation technique yielded complementary results at low fields. No evidence for the existence of a hole pocket at the point *L* in the Brillouin zone was found in either of the techniques. The use of superconducting solenoids with a maximum field of 120 kG resulted in data from all four the-

oretically predicted sheets of the Fermi surface. dHvA frequency measurements yielded central extremal areas and in some angular regions additional noncentral extremal areas which caused splitting of some dHvA frequency branches. In general, the experiments confirm the RAPW predictions that the Fermi surface of iridium consists of two large electron sheets centered at Γ and two small hole sheets centered at *X*. From a detailed comparison of the experimental and theoretical data for all the hole and electron sheets, it is apparent that the number of carriers associated with the three largest sheets is slightly larger than predicted while it is smaller for the X3 sheet. A slight change in the *sp-d* band separation¹² used in the calculations should correct this disagreement. The dHvA data agree with magnetoresistance data showing that the Fermi surface of iridium does not support open orbits and that iridium is an uncompensated metal.

ACKNOWLEDGMENTS

We wish to thank Dr. J. Vanderkooy, Dr. J. S. Moss, and Dr. I. M. Templeton for helpful comments. One of us (J.J.G.) is grateful to Dr. P. C. Eastman for his patronage and encouragement. Excellent technical assistance of the Physics Workshop is acknowledged. Thanks are also due to Dr. W. R. Datars of McMaster University for his generous permission to use facilities in his laboratory for some of the experiments. Extensive help from the Fermi-surface group at McMaster and in particular of A. Dunsworth is acknowledged.

[†]Research supported by grants from the National Research Council of Canada and the Department of University Affairs of the Province of Ontario.

*Province of Ontario Graduate Fellow. This research was completed in partial fulfillment of the Ph.D degree in Physics at the University of Waterloo. Present address: Université Paris-Sud, Centre d'Orsay, Laboratoire de Physique des Solides, Bâtiment 510, 91-Orsay, France.

¹K. Andres and M. A. Jensen, *Phys. Rev.* **165**, 533 (1968).

²A. I. Schindler and M. J. Rice, *Phys. Rev.* **164**, 759 (1967).

³M. P. Sarachik, *Phys. Rev.* **170**, 679 (1968).

⁴P. Lederer and D. L. Mills, *Phys. Rev.* **165**, 837 (1968).

⁵A. B. Kaiser and S. Doniach, *Intern. J. Magnetism* **1**, 11 (1971).

⁶K. H. Bennemann and J. W. Garland, *Intern. J. Magnetism* **1**, 97 (1971).

⁷A. P. Cracknell, *Advan. Phys.* **18**, 681 (1969); **20**, 1 (1971).

⁸J. J. Grodski, Ph.D. thesis (University of Waterloo, 1971) (unpublished).

⁹H. F. Schaake, *J. Less-Common Metals* **15**, 103 (1968).

¹⁰J. J. Grodski and A. E. Dixon, *Solid State Commun.* **7**, 735 (1969).

¹¹O. K. Andersen and A. R. Mackintosh, *Solid State Commun.* **6**, 285 (1968).

¹²O. K. Andersen, *Phys. Rev. B* **2**, 883 (1970).

¹³S. Hörnfeldt, A. Hammerström, K. Carrander, and G. Björck, *J. Phys. Chem. Solids* **32**, 753 (1971).

¹⁴N. V. Volkenshtein, V. A. Novoselov, and V. E. Startsev, *Zh. Eksperim. i Teor. Fiz.* **58**, 1609 (1970) [*Sov. Phys. JETP* **31**, 862 (1970)].

¹⁵N. V. Volkenshtein, V. A. Novoselov, V. E. Startsev, and Yu. N. Tsiovkin, *Zh. Eksperim. i Teor. Fiz.* **60**, 1773 (1971) [*Sov. Phys. JETP* **33**, 959 (1971)].

¹⁶S. J. Williamson, S. Foner, and R. A. Smith, *Phys. Rev.* **136**, 1065 (1964).

¹⁷O. K. Andersen, thesis (Technical University of Denmark, 1969) (unpublished).

¹⁸E. Fawcett and W. A. Reed, *Phys. Rev.* **131**, 2463 (1963).

¹⁹Koch-Light Laboratories, Colnbrook, Buckinghamshire, England.

²⁰Preparation of Platinum Metals for Metallography, Mond Nickel Co. Ltd., England (unpublished).

²¹E. A. Wood, *Crystal Orientation Manual* (Columbia U.P., New York, 1963), p. 20.

²²P. T. Coleridge, A. A. M. Croxon, G. B. Scott, and

- I. M. Templeton, *J. Phys.* E 4, 414 (1971).
- ²³A. B. Pippard, *The Dynamics of Conduction Electrons* (Gordon and Breach, New York, 1965), p. 21.
- ²⁴G. B. Scott, M. Springford, and J. R. Stockton, *J. Phys.* E 1, 925 (1968).
- ²⁵J. Vanderkooy and W. R. Datars, *Phys. Rev.* 156, 671 (1967).
- ²⁶Model 1411, Weston Instruments Division, Newark, N. J. 07114.
- ²⁷A. Goldstein, S. J. Williamson, and S. Foner, *Rev. Sci. Instr.* 36, 1356 (1965).
- ²⁸R. W. Stark and L. R. Windmiller, *Cryogenics* 8, 272 (1968).
- ²⁹Model 2T60-1110 with a modified S-10 speed controller, G. H. Heller, Las Vegas, Nev. 89114.
- ³⁰R. G. Poulsen, J. S. Moss, and W. R. Datars, *Phys. Rev. B* 3, 3107 (1971).
- ³¹A. C. Thorsen and T. G. Berlincourt, *Rev. Sci. Instr.* 34, 435 (1963).
- ³²Molykote Z, Dow Corning Corp., Midland, Mich. 48640.
- ³³E. R. Andrew, I. Roberts, and R. C. Gupta, *J. Sci. Instr.* 43, 936 (1966).
- ³⁴Adhesive and insulating varnish No. 7031, General Electric, Schenectady, N. Y. 12305.
- ³⁵Type FA-135-173, Wallace & Tiernan, 25 Main St., Belleville, N. J. 07109.
- ³⁶B. R. Watts, *Proc. Roy. Soc. (London)* A282, 521 (1964).
- ³⁷J. B. Ketterson and L. R. Windmiller, *Phys. Rev. B* 2, 4813 (1970).
- ³⁸L. R. Windmiller, J. B. Ketterson, and S. Hörnfeldt, *Phys. Rev. B* 3, 4213 (1971).
- ³⁹J. B. Ketterson, L. R. Windmiller, and S. Hörnfeldt, *Phys. Letters* 26A, 115 (1968).
- ⁴⁰J. S. Lass and A. B. Pippard, *J. Phys.* E 3, 137 (1970).
- ⁴¹P. B. Visscher and L. M. Falicov, *Phys. Rev. B* 2, 1518 (1970).

PHYSICAL REVIEW B

VOLUME 6, NUMBER 4

15 AUGUST 1972

Electronic Structure of Noble-Metal-Noble-Metal Alloys[†]

David Beaglehole*

Physics Department, University of Maryland, College Park, Maryland 20742

and

Erich Erlbach[‡]*City College of the City University of New York, Convent Ave., New York 10031*

(Received 3 December 1971)

We describe optical studies of dilute noble-metal-noble-metal alloys. A differential technique compared the reflectance of the alloy with the reflectance of the pure metal and measured a quantity proportional to just the difference in reflectance. The method was particularly sensitive to small changes in reflectances and could be used to study very dilute alloys—the alloys here were between $\frac{1}{10}$ - and 3-at. % impurity concentration. The measurements indicated that the noble alloys are of two types. In copper-gold and silver-gold alloys the electron energy bands shift smoothly as the concentration varies. The rates and directions of shifts are determined not only by differences in the host and impurity potentials, but also by the changes in lattice constant, and we emphasize the importance of the latter. In contrast, in copper-silver alloys separate host and impurity d bands are formed.

I. INTRODUCTION

While the electronic structure of metal crystals is now fairly well understood, the theory of alloys is still rudimentary. The difficulty is that common to all disordered systems (liquid, amorphous, and alloys)—the difficulty of including the correlation effects involved in a random distribution of atoms. In two limits, however, the theory is well based.¹ In the weak-perturbation limit, when the components disturb each other only slightly when mixed, the energy levels should move smoothly from those characteristic of one component to those characteristic of the other as the concentration varies. In the strong-perturbation limit, when the energies

and wave functions of the two components are very different, the electrons should maintain their individual character and form localized or resonant states. Recently, the coherent-potential theory²⁻⁴ has provided a link between these two extreme limits, though the theory at present is based on rather simple assumptions concerning the interaction of electrons on different sites.

Experimentally it is of interest to study how various alloy systems fit into the range of perturbation behaviors. Optical experiments are particularly useful, since they measure the excitation of electrons between allowed energy levels and can distinguish between the weak- or strong-perturbation situations and measure changes in energy levels.